Bayat *et al. Adv. Model. and Simul. in Eng. Sci.(2018)5:10*
https://doi.org/10.1186/s40323-018-0103-x

Advanced Modeling and Simulation in Engineering Sciences

RESEARCH ARTICLE Open Access

On the use of reduced integration in combination with discontinuous Galerkin discretization: application to volumetric and shear locking problems

Hamid Reza Bayat*, Stephan Wulfinghoff, Steffen Kastian and Stefanie Reese

*Correspondence: hamid.reza.bayat@rwth-aachen.de
Institute of Applied Mechanics, RWTH Aachen University, 52074 Aachen, Germany

Abstract

In the present work, the discontinuous Galerkin (DG) method is applied to linear elasticity for two-dimensional and three-dimensional settings. A locking-free element formulation based on reduced integration and physically-based hourglass stabilization (Q1SP) is coupled for the first time with the DG framework. The incomplete interior penalty Galerkin method is chosen, being one example of different variations of DG methods. Several 2D and 3D typical benchmark problems of linear elasticity are investigated. A selection of numerical integration schemes for the boundary terms is presented, namely reduced and mixed integration schemes. The treatment of the surface terms by means of different rules of integration shows a significant influence on the performance of the resulting DG method in combination with the standard Q1 element. This intelligent treatment of the surface part leads to a DG variant with very good convergence properties.

Keywords: Discontinuous Galerkin, Reduced integration, Incompressibility, Linear elasticity

Introduction

In the last decades, finite element-based discontinuous Galerkin methods (DG) have been established as good alternative to standard continuous finite element formulations.

Reed and Hill [1] (see also LeSaint and Raviart [2]) were among the first authors to introduce a DG method. The method was set up for hyperbolic PDEs—to solve the problem of neutron transport. It was observed that the discontinuities between the subdomains may lead to non-uniqueness of the discrete solution. In order to stabilize the solution, a penalty term due to Nitsche [3] is frequently added on the element boundaries. After its initialization, there was an increasing interest in DG methods for hyperbolic and nearly hyperbolic problems, see for example the work of Johnson and Pitkäranta [4] as well as [5–7]. Douglas and Dupont [8], Wheeler [9] and Arnold [10] introduced the interior penalty (IP) variant of the DG method to extend the range of applicability of the method (see also [11–13]). The first application of DG for a fourth order problem was carried out by Baker [14]. Bassi and Rebay [15] solved the compressible Navier-Stokes equations by a DG method.

Springer Open

The latter work was further extended to time-dependent convection-diffusion systems by Cockburn and Shu [16] who introduced the so-called "local" discontinuous Galerkin method. Another application of a DG method for diffusion problems was presented by Oden and Bauman [17,18]. An overview of the application of the DG method for elliptic problems can be found in [19]. Detailed reviews on the development of DG methods can be found in [20,21].

Applications of DG methods are predominantly found in fluid/gas dynamics [15,17,22], compressible [23,24]/incompressible flows [25,26], magneto-hydrodynamics [27], granular flows [28], viscoplastic crack growth and chemical transport [29]. Recently, there has been increasing interest in the application of DG methods in solid mechanics. In 2002, Engel et al. [30] made a comparison between continuous and discontinuous Galerkin methods to solve fourth-order elliptic problems such as they occur in thin beams and plates, and strain-gradient elasticity. A further extension of the latter work to strain gradient-dependent damage was carried out by Wells et al. [31] and Morali et al. [32]. Space-time discretization was applied in linear-elastic DG methods after Huang and Costanzo [33,34] had introduced it. A discontinuous Galerkin time discretization for elasto-plasticity was proposed by Alberty and Cartensen [35]. Furthermore, Mergheim et al. [36] applied a DG method to avoid unphysical use of penalty terms in crack propagation problems. In addition, Alipour et al. [37] introduced the concept of control points in hybrid DG methods for problems of geometrically nonlinear crystal plasticity.

Discontinuous Galerkin methods turned out to be an alternative to continuous finite element technologies to treat locking phenomena. In the case of volumetric locking, Hansbo and Larson [38,39], Wihler [40] and Di Pietro and Nicaise [41] proved that their DG methods are locking-free for linear elasticity. Ten Eyck and Lew [42] investigated the latter problem for nonlinear elasticity as well. Concerning shear locking, the problem of Timoshenko beams was analyzed and discussed in the work of Celiker et al. [43]. Wulfinghoff et al. [44] introduced a low-order hybrid DG method for large deformations and proved that it is free of shear and volumetric locking. In continuous Galerkin (CG) formulations, Reese et al. [45] introduced a new 2D low-order element with reduced integration and hourglass stabilization (Q1SP) for nonlinear elasticity (see also [46–48]). The latter element performs very well and is free of both, shear and volumetric locking. Later, Reese et al. [49] found an equivalence between the aforementioned element formulation (Q1SP) and the HDG method of Wulfinghoff et al. [44]. As a result, the penalty scalar parameter is defined as a matrix and can be determined analytically.

In the present work, different reduced integration techniques are investigated regarding their potential to reduce volumetric and shear locking phenomena for the case of linear elasticity. In addition to that, a locking free formulation of Reese (see [48,50]) that has originally been proposed for the continuous FE method, is combined for the first time with the discontinuous setting.

The structure of the paper is as follows. First, the formulation of the DG method including its strong and weak form and its discretization is explained. Further emphasis is put on the integration schemes and the motivation to apply them in this work. "Examples" gives different 2D and 3D examples for cases, in which shear and volumetric locking phenomena are highly pronounced. Finally, the application of DG elements with Q1/Q1SP elements and their performance in locking problems are discussed.

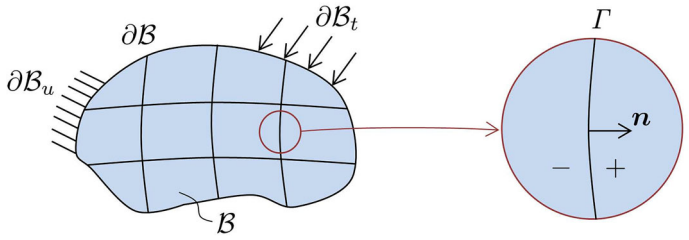

Fig. 1 Discontinuities within the body

DG formulations

The various DG methods differ in the terms included in the discrete weak form [19]. Accordingly, also different properties are found. Here, the unsymmetric incomplete interior penalty Galerkin method (IIPG) is used as basis and discussed later. In the following, the strong form of the linear momentum balance will be introduced, followed by the weak form. Next, the discretization method and the numerical integration schemes will be explained and discussed.

Strong form

A body $\mathcal{B}$ with boundary $\partial\mathcal{B}$ is considered, as illustrated in Fig. 1. The prescribed displacement $\boldsymbol{u}^p$ and the prescribed traction $\boldsymbol{t}^p$ act on the Dirichlet boundary $\partial\mathcal{B}_u$ and the Neumann boundary $\partial\mathcal{B}_t$, respectively. Additionally, the conditions $\partial\mathcal{B}_u \bigcup \partial\mathcal{B}_t = \partial\mathcal{B}$ and $\partial\mathcal{B}_u \bigcap \partial\mathcal{B}_t = 0$ hold.

Thus, the strong form of the quasi-static linear momentum balance and the related boundary conditions are given by

$$\operatorname{div}(\boldsymbol{\sigma}) + \boldsymbol{f} = \boldsymbol{0}, \tag{1}$$

$$\boldsymbol{u} = \boldsymbol{u}^p \quad \text{on} \quad \partial\mathcal{B}_u,$$

$$\boldsymbol{\sigma}\,\boldsymbol{n} = \boldsymbol{t}^p \quad \text{on} \quad \partial\mathcal{B}_t, \tag{2}$$

where $\boldsymbol{\sigma}$ is the Cauchy stress tensor and $\mathbf{f}$ represents the body force vector. Since the material is linear elastic, Hooke's law

$$\boldsymbol{\sigma} = \boldsymbol{C} : \boldsymbol{\varepsilon}, \tag{3}$$

is applied, where $\boldsymbol{C}$ represents the fourth order elasticity tensor. The quantity $\boldsymbol{\varepsilon}$ is the infinitesimal strain tensor being defined by

$$\boldsymbol{\varepsilon}(\boldsymbol{x}) = \operatorname{sym}(\operatorname{grad}(\boldsymbol{u})). \tag{4}$$

In contrast to continuous Galerkin approaches, DG methods allow discontinuities on the internal boundaries Γ as depicted in Fig. 1.

In this simple example (Fig. 1), these discontinuities divide the body $\mathcal{B}$ into several subdomains. On each side of Γ, the body is denoted by $-$ and $+$ with respect to the direction of the normal vector $\boldsymbol{n}$ which points from $-$ to $+$. There may be discontinuities in the displacement field $\boldsymbol{u}$, the strain tensor $\boldsymbol{\varepsilon}$ and the stress tensor $\boldsymbol{\sigma}$ as well. In general,

the body $\mathcal{B}$ can contain a finite number of discontinuities Γ that divide the body $\mathcal{B}$ into large number of subdomains. Please note that the surface Γ is not related to any physical interface. Accordingly, we define jump $[\![\cdot]\!]$ and average $\{\cdot\}$ values as shown below:

$$\begin{aligned} [\![\boldsymbol{u}]\!] &= (\boldsymbol{u}^{+}|_{\Gamma} - \boldsymbol{u}^{-}|_{\Gamma}), \\ \{\boldsymbol{u}\} &= \frac{1}{2}(\boldsymbol{u}^{+}|_{\Gamma} + \boldsymbol{u}^{-}|_{\Gamma}). \end{aligned} \tag{5}$$

Finally, it is noted that the continuous solution satisfies the following equations:

$$\begin{aligned} [\![\boldsymbol{u}]\!] &= \mathbf{0} \quad \text{on} \quad \Gamma, \\ [\![\boldsymbol{\sigma}]\!]\,\mathbf{n} &= \mathbf{0} \quad \text{on} \quad \Gamma. \end{aligned} \tag{6}$$

Weak form

Having the equilibrium equation and boundary conditions (BCs) at hand, one derives the weak form by first multiplying the strong form with a test function $\delta\boldsymbol{u}$ and then integrating over the considered domain. In the spirit of Nitsche's method [3], a penalty term is added to assure stability of the solution (third term on the left hand side of Eq. 7). One should bear in mind that the addition of this term does not alter the continuous solution since according to Eq. 6, the jump in the displacement field vanishes. As a result, one obtains:

$$\begin{aligned} &\int_{\mathcal{B}} \boldsymbol{\sigma} : \delta\boldsymbol{\varepsilon}\, dV + \int_{\Gamma} [\![\delta\boldsymbol{u}]\!] \cdot \{\boldsymbol{\sigma}\}\, \boldsymbol{n}\, d\Gamma + \beta \int_{\Gamma} [\![\boldsymbol{u}]\!] \cdot \{\delta\boldsymbol{\sigma}\}\, \boldsymbol{n}\, d\Gamma + \int_{\Gamma} \theta\, [\![\delta\boldsymbol{u}]\!] \cdot [\![\boldsymbol{u}]\!]\, d\Gamma \\ &\quad = \int_{\mathcal{B}} \boldsymbol{f} \cdot \delta\boldsymbol{u}\, dV + \int_{\partial\mathcal{B}_t} \boldsymbol{t}^{p} \cdot \delta\boldsymbol{u}\, dA, \end{aligned} \tag{7}$$

where $\theta = \eta E/h$ [N/m^3] is a penalty parameter which depends on the Young's modulus (E), the mesh size of the structure (h) and a sufficiently large positive number (η) ([36,38,51]). The scalar value β can vary between 0, -1 and 1, leading to different interior penalty Galerkin methods, namely incomplete (IIPG), non-symmetric (NIPG) and symmetric (SIPG), respectively. A detailed overview of the DG methods can be found in [19]. In the present work, the incomplete interior penalty Galerkin method is applied which is non-symmetric due to the missing dual consistency term. On the other hand, the implementation of the method is less elaborate. In addition, due to the consistency error resulting from the omitted term, super-penalization of this method can be applied to obtain optimal error estimates [19]. The super-penalty technique can lead DG to perform like conforming methods. Nonetheless, in this work, the super-penalty approach compensates for the reduced integration schemes and delivers a locking-free behavior unlike continuous Galerkin formulations.

Discretization

After transferring the strong form into the weak form, the next step is to discretize the body $\mathcal{B}$ into finite elements. Using standard isoparametric elements $\mathcal{B}_e$, the discretization is given by

$$\mathcal{B} = \bigcup_{e} \mathcal{B}_e. \tag{8}$$

The position vector $\boldsymbol{x}^h$, the displacement field $\boldsymbol{u}^h$ and the test function $\delta\boldsymbol{u}^h$ are interpolated within each element. In the 2D settings, quadrilateral elements are applied using bilinear shape functions, while in 3D case, hexahedral elements with trilinear shape functions are used:

$$\begin{aligned}\boldsymbol{x}^h(\xi,\eta) &= \sum_{I=1}^{n_{en}} N^I(\xi,\eta)\boldsymbol{x}_I,\\ \boldsymbol{u}^h(\xi,\eta) &= \sum_{I=1}^{n_{en}} N^I(\xi,\eta)\boldsymbol{u}_I,\\ \delta\boldsymbol{u}^h(\xi,\eta) &= \sum_{I=1}^{n_{en}} N^I(\xi,\eta)\delta\boldsymbol{u}_I,\end{aligned} \tag{9}$$

where (ξ,η) are the coordinates in the reference element and n_{en} is the element node number. The latter can vary between 4 and 8 for the 2D and 3D elements, respectively . As the degrees of freedom of the individual elements in DG discretization are decoupled, each $\boldsymbol{u}_I$ is related only to one element at a time. Accordingly, the jump and the average of the displacement must be discretized as follows:

$$\begin{aligned}[[\boldsymbol{u}^h]]|_{\Gamma_e} &= \sum_{I=1}^{n_{en}^+} N^I|_{\Gamma_e}(\xi,\eta)\boldsymbol{u}_I{}^+ - \sum_{I=1}^{n_{en}^-} N^I|_{\Gamma_e}(\xi,\eta)\boldsymbol{u}_I{}^-,\\ \{\boldsymbol{u}^h\}|_{\Gamma_e} &= \frac{1}{2}\left[\sum_{I=1}^{n_{en}^+} N^I|_{\Gamma_e}(\xi,\eta)\boldsymbol{u}_I{}^+ + \sum_{I=1}^{n_{en}^-} N^I|_{\Gamma_e}(\xi,\eta)\boldsymbol{u}_I{}^-\right],\end{aligned} \tag{10}$$

where n_{en}^+ (n_{en}^-) represents the number of element nodes on the "positive" ("negative") side of the interface Γ_e. The jump and average of the virtual displacement $\delta\boldsymbol{u}^h$ is derived in the same manner. The strain tensor $\boldsymbol{\varepsilon}^h$ is computed according to Eq. 4, using the derivatives of the shape functions. In this variant of the DG method, we also need to introduce the average stress $\{\boldsymbol{\sigma}^h\}$ along Γ:

$$\{\boldsymbol{\sigma}^h\} := \frac{1}{2}[\boldsymbol{\sigma}^{h+}|_{\Gamma_e} - \boldsymbol{\sigma}^{h-}|_{\Gamma_e}]. \tag{11}$$

For the sake of simplicity, we avoid writing the approximation superscript "h" from here onward. Recalling Hooke's law (Eq. 3) and introducing the $\boldsymbol{B}$-operator to interpolate the linearized strain tensor $\boldsymbol{\varepsilon}$, we can rewrite the average Cauchy stress as:

$$\{\boldsymbol{\sigma}\}|_{\Gamma_e} = \frac{1}{2}\left[\sum_{I=1}^{n_{en}^+} C^+B^I|_{\Gamma_e}\ \boldsymbol{u}_I^+ + \sum_{I=1}^{n_{en}^-} C^-B^I|_{\Gamma_e}\ \boldsymbol{u}_I^-\right] \tag{12}$$

Introducing the same quantities in matrix notation for the formation of the residual vectors and stiffness matrices, one rewrites the jump and average values as follows:

$$
\begin{aligned}
[\![\boldsymbol{u}]\!] &= \begin{bmatrix} \mathbf{N}^+ & -\mathbf{N}^- \end{bmatrix} \begin{bmatrix} \boldsymbol{u}_d^+ \\ \boldsymbol{u}_d^- \end{bmatrix} \\
\{\boldsymbol{u}\} &= \frac{1}{2} \begin{bmatrix} \mathbf{N}^+ & \mathbf{N}^- \end{bmatrix} \begin{bmatrix} \boldsymbol{u}_d^+ \\ \boldsymbol{u}_d^- \end{bmatrix} \\
\{\boldsymbol{\sigma}\} &= \frac{1}{2} \begin{bmatrix} \mathbf{C}^+\mathbf{B}^+ & \mathbf{C}^-\mathbf{B}^- \end{bmatrix} \begin{bmatrix} \boldsymbol{u}_d^+ \\ \boldsymbol{u}_d^- \end{bmatrix}
\end{aligned} \tag{13}
$$

where the subscript d refers to terms evaluated on the discontinuity Γ_e. Substituting the average and jump terms in (7), one can obtain the discontinuous part of the discretized weak formulation at element level:

$$
\begin{aligned}
&\begin{bmatrix} \delta\boldsymbol{u}_d^{+T} & \delta\boldsymbol{u}_d^{-T} \end{bmatrix} \int_{\Gamma_e} \frac{1}{2} \begin{pmatrix} \mathbf{N}^{+T} \\ -\mathbf{N}^{-T} \end{pmatrix} \mathbf{n} \begin{bmatrix} \mathbf{C}^+\mathbf{B}^+ & \mathbf{C}^-\mathbf{B}^- \end{bmatrix} d\Gamma_e \begin{bmatrix} \boldsymbol{u}_d^+ \\ \boldsymbol{u}_d^- \end{bmatrix} \\
&+ \begin{bmatrix} \delta\boldsymbol{u}_d^{+T} & \delta\boldsymbol{u}_d^{-T} \end{bmatrix} \int_{\Gamma_e} \theta \begin{pmatrix} \mathbf{N}^{+T} \\ -\mathbf{N}^{-T} \end{pmatrix} \begin{bmatrix} \mathbf{N}^+ & -\mathbf{N}^- \end{bmatrix} d\Gamma_e \begin{bmatrix} \boldsymbol{u}_d^+ \\ \boldsymbol{u}_d^- \end{bmatrix}
\end{aligned} \tag{14}
$$

Deriving this relation with respect to $\delta\boldsymbol{u}$, once can get the residual $\boldsymbol{R}_e^{disc}$ for the discontinuous part:

$$
\begin{aligned}
\boldsymbol{R}_e^{disc} = &\int_{\Gamma_e} \frac{1}{2} \begin{pmatrix} \mathbf{N}^{+T} \\ -\mathbf{N}^{-T} \end{pmatrix} \mathbf{n} \begin{bmatrix} \mathbf{C}^+\mathbf{B}^+ & \mathbf{C}^-\mathbf{B}^- \end{bmatrix} d\Gamma_e \begin{bmatrix} \boldsymbol{u}_d^+ \\ \boldsymbol{u}_d^- \end{bmatrix} \\
&+ \int_{\Gamma_e} \theta \begin{pmatrix} \mathbf{N}^{+T} \\ -\mathbf{N}^{-T} \end{pmatrix} \begin{bmatrix} \mathbf{N}^+ & -\mathbf{N}^- \end{bmatrix} d\Gamma_e \begin{bmatrix} \boldsymbol{u}_d^+ \\ \boldsymbol{u}_d^- \end{bmatrix}.
\end{aligned} \tag{15}
$$

A successive derivation with respect to $\boldsymbol{u}$ yields the dG element stiffness matrix $\boldsymbol{K}_e^{disc}$, which is given by the sum of two integrals $\boldsymbol{K}_{e_1}^{disc}$ and $\boldsymbol{K}_{e_2}^{disc}$, where:

$$
\begin{aligned}
\boldsymbol{K}_{e_1}^{disc} &= \int_{\Gamma_e} \frac{1}{2} \begin{pmatrix} \mathbf{N}^{+T} \\ -\mathbf{N}^{-T} \end{pmatrix} \mathbf{n} \begin{bmatrix} \mathbf{C}^+\mathbf{B}^+ & \mathbf{C}^-\mathbf{B}^- \end{bmatrix} d\Gamma_e \\
\boldsymbol{K}_{e_2}^{disc} &= \int_{\Gamma_e} \theta \begin{pmatrix} \mathbf{N}^{+T} \\ -\mathbf{N}^{-T} \end{pmatrix} \begin{bmatrix} \mathbf{N}^+ & -\mathbf{N}^- \end{bmatrix} d\Gamma_e.
\end{aligned} \tag{16}
$$

Numerical integration

We divide the left hand side of Eq. 7 into two parts. The first one being related to the area integral is evaluated using integration points in the interior of the elements (first integral). The second part being associated to the boundary integrals is evaluated at integration points on the element edges (second and forth integrals). The latter one consists of two integrals, namely the DG and the penalty terms. Please note that the third term of Eq. 7 is not considered in this work since we are applying the IIPG method.

For the evaluation of the first part, Q1 and Q1SP [46,48] elements are used. In the 2D setting, the Q1 element is a standard four-node quadrilateral (Q) element with four integration points and shape functions of polynomial order one (1), whereas the Q1SP element possesses only one integration point in the element center combined with a special hourglass stabilization (S) technique which applies the equivalent parallelogram (P) concept and is thus free of volumetric and shear locking (see [50] for more information). In the 3D case, the Q1 and Q1SP elements are hexahedrals with trilinear shape functions. While Q1

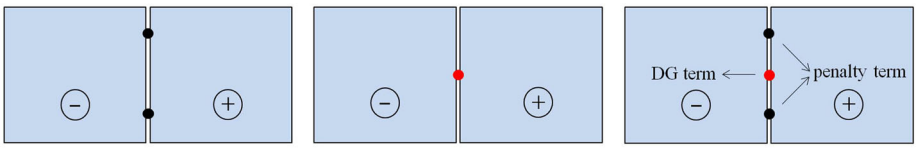

Fig. 2 DG interface with full (left), reduced (middle) and mixed (right) integration schemes for 2D elements

elements possess eight integration points, Q1SP benefits from reduced integration (only one in the middle) and an hourglass stabilization approach as well.

The evaluation of the second part is performed by applying the DG discretization for the DG and penalty terms. The standard Gaussian quadrature implies full integration (two Gauss points in 2D and 4 Gauss points in 3D) on the interior element boundaries for both DG and penalty terms (see Fig. 2 (left)). From now on, we illustrate the numerical schemes only for the 2D case. In analogy, the same concepts are applied in the 3D setting.

However, having two integration points on the interior element boundaries for both DG and penalty terms results in a high total number of quadrature points. This implies that an element surrounded by four other elements will have four quadrature points in the area integral and eight for each of the DG and penalty terms on the entire element boundaries. It is well-known that this may lead to an artificial stiffening of the element behavior known as "locking phenomenon".

To remedy this problem (locking), the first concept (mixed integration) is to evaluate the DG term only in the middle of the discontinuity (reduced integration) but the penalty term still on two Gauss points (full integration). The latter results in a penalization of the relative rotation between two adjacent elements. Mixed integration is illustrated in Fig. 2 (right).

In the second approach, only one integration point in the middle of the discontinuity is introduced for both, DG and penalty terms of the Eq. 7 (see Fig. 2 (middle)). This will reduce not only the number of the constraints, but also the calculation costs.

Examples

In this section, we investigate five well-known examples, namely Cook's membrane, the bending of a thin beam/a thin plate (3D) and a block (2D/3D) under compression, where volumetric and shear locking can be observed for conventional Q1 elements. The simulations are done using the finite element analysis program FEAP [52] and the mesh generation is carried out by MATLAB® and FEAP.

Cook's membrane

Cook's membrane is commonly investigated to explore the element behavior in a mixed situation where both bending and near-incompressibility occur [48]. Figure 3 depicts the geometry and the boundary conditions of the problem. The body is fixed on the left hand side. A vertical load is applied on the right hand side. Poisson's ratio is set to $\nu = 0.4999$, modeling near-incompressibility. Additionally, Young's modulus is given by $E = 240.565$ MPa.

The aim of this example is to investigate the locking behavior and to make a comparison between the standard continuous finite element and DG methods. Consequently, the

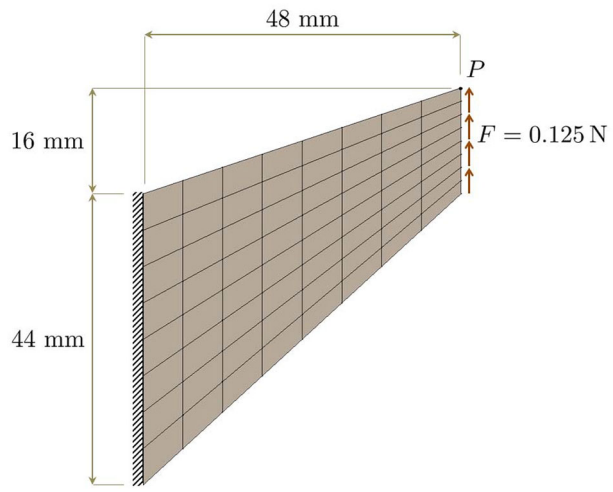

Fig. 3 Cook's membrane, geometry, boundary conditions, loading and discretization

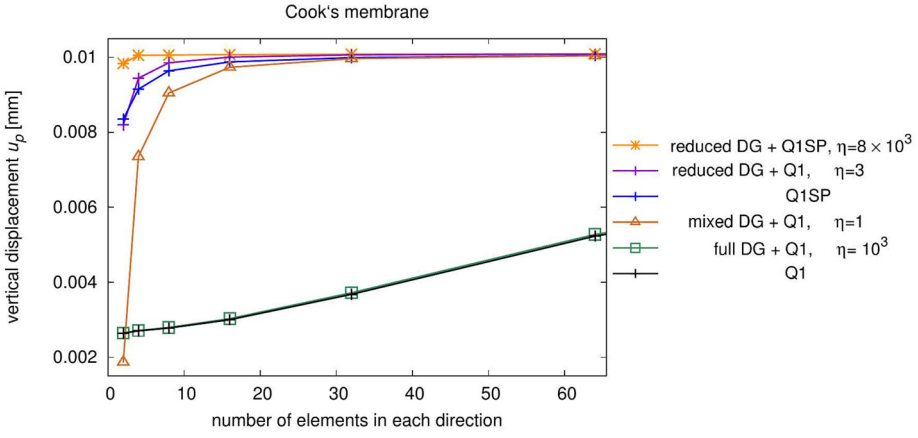

Fig. 4 Vertical displacement of the point *P* as a function of the number of elements in each direction for Q1, Q1SP, DG and their combinations

simulations are carried out for different elements, namely the continuous Q1 and Q1SP elements as well as the related discontinuous Galerkin counterparts. The "mixture" of DG and the locking-free element Q1SP is used to investigate whether there is an improvement in the convergence with respect to element size. This convergence is checked by dividing each side of the geometry into equal numbers of elements to make the mesh finer (see Fig. 3 for 2 by 2 elements). The vertical displacement u_P of the point P is studied for every mesh refinement.

According to Fig. 4, the standard Q1 element exhibits severe volumetric locking. On the other hand, application of DG with full integration does not have any influence on its convergence. On the contrary, the Q1SP element is already close to the converged solution with 16 elements in each direction. The use of the reduced DG method improves the convergence of the Q1 element significantly being even faster than continuous Q1SP. This improvement is pronounced particularly in case of the discontinuous version of the Q1SP element (reduced DG + Q1SP). Besides, mixed DG in combination with the Q1

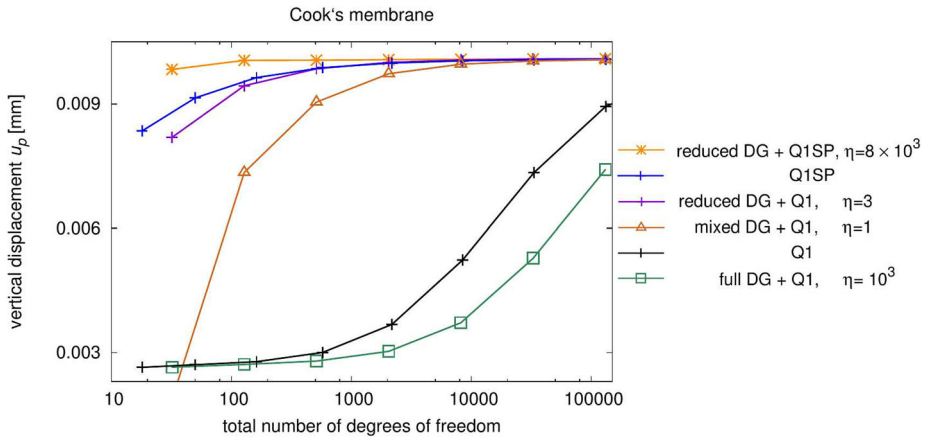

Fig. 5 Vertical displacement of the point *P* as a function of the total number of degrees of freedom for Q1, Q1SP, DG and their combinations

element shows also a very good convergence in comparison to Q1 and its discontinuous version with full integration. However, it should be kept in mind, that for a given number of elements, the number of degrees of freedom is significantly larger than that of the continuous discretization.

In spite of this fact, the discontinuous variants still converge better in comparison to the continuous elements with respect to the total number of degrees of freedom as illustrated in Fig. 5. The figure shows that the combination of DG and Q1SP results in the best convergence. Moreover, Q1SP shows a slightly better convergence than the discontinuous Q1 element with reduced integration. The worst convergence belongs to the discontinuous Q1 with fully integrated DG due to the increase of degrees of freedom.

In order to find the appropriate penalty value $\theta = \eta E/h$ [N/m^3], one needs to choose the η value sufficiently large to ensure a sufficient stabilization [19]. However, a too large θ value leads to an over-penalization of the displacement jumps. This causes locking again since the DG method will behave like the continuous Galerkin method. It should be noted that the high value of $\eta = 8 \times 10^3$ in the combination of reduced DG and the Q1SP element is due to the fact that both aforementioned elements have reduced integration points and thus need a higher penalization value to get stabilized. Nevertheless, the determination of the penalty parameter is still an elaborate task.

Thin beam under shear loading

In this example, a thin beam [47] as depicted in Fig. 6 is loaded by a vertical upward force on its right upper corner. Young's modulus is set to $E = 16800$ MPa and Poisson's ratio is chosen to be $\nu = 0.4$. The beam is fixed at the left hand side and the vertical displacement of the point A, u_A, is investigated in order to evaluate the mesh convergence behavior. To this end, the following different mesh resolutions are considered: $1 * 10,\ 2 * 20,\ 4 * 40,\ 8 * 80$, and $16 * 160$.

As can be seen in Fig. 7, the Q1 element suffers from shear locking as expected due to the high ratio of the element lengths. Similar to Cook's membrane, the Q1 element with full integration DG has the slowest convergence. On the contrary, Q1SP and its discontinuous variation with mixed integration show the best convergence behavior, giving

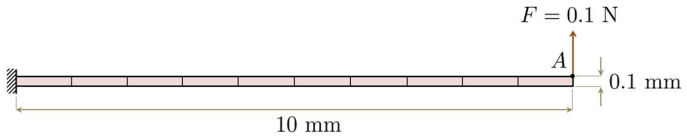

Fig. 6 Thin beam, geometry, boundary conditions, loading and discretization

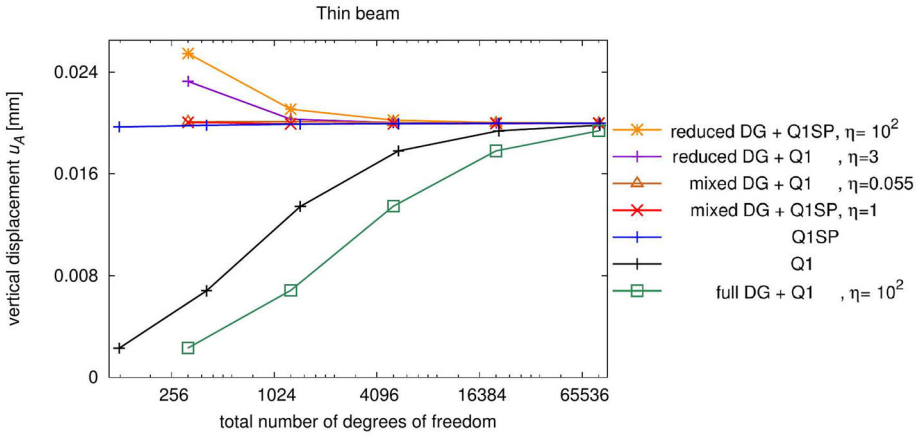

Fig. 7 Vertical displacement of the point *P* as a function of the total number of degrees of freedom for Q1, Q1SP, DG and their combinations

very good results already with a very small number of degrees of freedom. in this case the discontinuous Q1SP with reduced DG is still very good, however not the best. Unlike Cook's membrane, the discontinuous Q1 element with reduced DG outperforms the latter combination.

The choice of the positive constant η plays a crucial role in the convergence rate. Having chosen the best value, one can reach converged solution irrespective of the mesh size.

2D block under compression

The third example examines the behavior of the DG method in compression problems. Consequently, a block under compression from [45] is considered. Figure 8 illustrates the geometry, boundary conditions and the loading. It is fixed in vertical direction at the bottom and in the horizontal direction on the top. a distributed load of $p_0 = 0.02$ MPa acts on the top as depicted in Fig. 8. The material parameters are the same as those of Cook's membrane. Thus near-incompressible material is considered in this example as well. The vertical displacement of the point A, u_A is investigated. Due to the symmetry condition, half of the block is divided into 2, 4, 8, 16,... elements on each of its sides simultaneously.

In this example (Fig. 9), the same as the previous examples, the discontinuous Q1 with DG full integration and the continuous Q1 are the slowest and second slowest converging elements, respectively. Continuous Q1SP element converges very fast. However, the combination of Q1SP with DG elements (both reduced and mixed) results in the fastest convergence and improves the performance of Q1SP. On the other hand, the mixed and reduced discontinuous Q1 elements also show very good convergence. In this com-

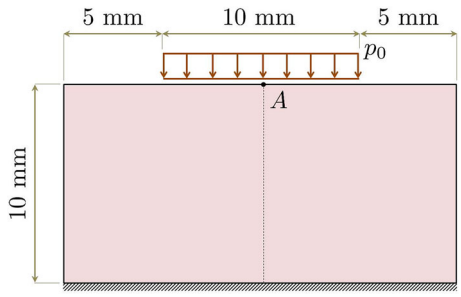

Fig. 8 Thin beam, geometry, boundary conditions, loading and discretization

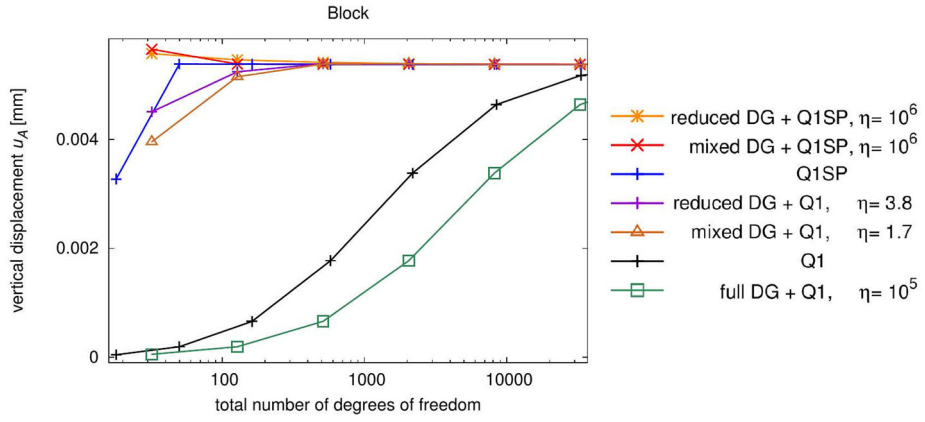

Fig. 9 Vertical displacement of the point A as a function of the total number of degrees of freedom for Q1, Q1SP, DG and their combinations

pression example the constant η must be set to a high value to guarantee a converged solution.

3D block under compression

The extension of the 2D block to the 3D setting is investigated here. The material parameters E and ν are set to 4.82926 MPa and 0.499 (nearly incompressible), respectively. The horizontal degrees of freedom are constrained at the top whereas only the vertical degrees of freedom are fixed at the bottom of the block. In addition, a compressive distributed load of 0.003 MPa is applied on the middle surface of the upper face of the block. The discretization of the block is established similar to the 2D block by considering the quarter symmetry and simultaneous division of block in all three directions. Figure 10 illustrates the geometry, boundary conditions, discretization and the loading in this example. Eventually, we investigate the vertical displacement of the point P.

As it is depicted in Fig. 11, DG elements in combination with Q1 elements reduce the locking effects provided that reduced integration on the boundary terms is applied. Otherwise, severe locking is observed in presence of full integration. Applying discontinuous elements in 2D cases resulted already in a considerable increase in the number of degrees of freedom. This problem is highly pronounced in 3D examples. This is illustrated in Fig. 11, where a comparison between the convergence rate once with respect to the num-

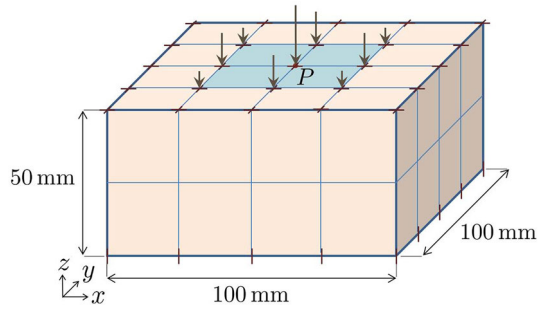

Fig. 10 3D block, geometry, boundary conditions, loading and discretization

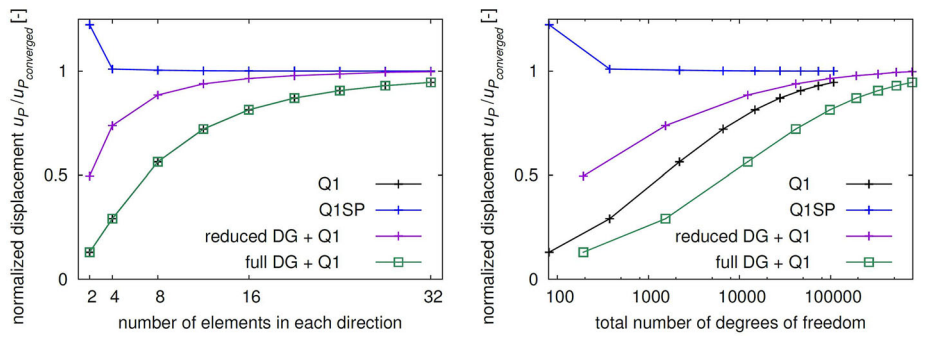

Fig. 11 Normalized vertical displacement of the point P in the 3D block as a function of the number of elements in each direction (left) and total degrees of freedom (right) for Q1, Q1SP, DG and their combinations with $\eta = 10^7$

ber of elements (left) and once with respect to the number of degrees of freedom (right) is made.

3D thin plate

To investigate shear locking in the 3D setting, a thin plate is considered in this section. Young's modulus and Poisson's ratio are set to 250 MPa and 0.3, respectively. A distributed load acts on the upper surface of the plate while it is fixed on its surrounding sides. The number of the elements in thickness direction is set to 4, whereas the number of elements in other directions are doubled in each mesh refinement. The geometry, boundary conditions, discretization and loading are depicted in Fig. 12. The vertical displacement of the point P is investigated.

Due to the thin geometry of the structure and the loading, shear locking is observed in the continuous Q1 and its discontinuous counterpart with full integration (see Fig. 13). The best convergence in this example belongs to the Q1SP element, however. It is noticeable that, in analogy to the previous example, application of DG in 3D settings brings about a huge increase in the number of degrees of freedom, which is computationally inefficient. Nonetheless, discontinuous Q1 elements with reduced integration on interfaces perform still considerably better than the continuous Q1 elements in terms of total number of degrees of freedom.

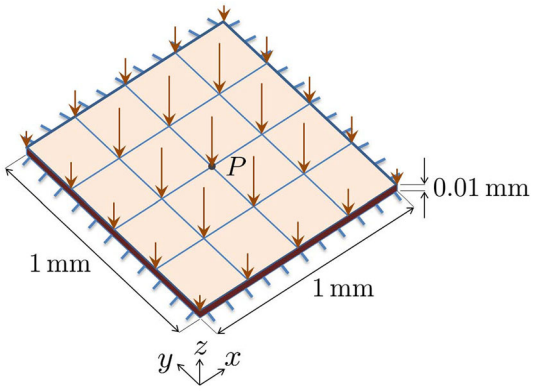

Fig. 12 Thin plate, geometry, boundary conditions, loading and discretization

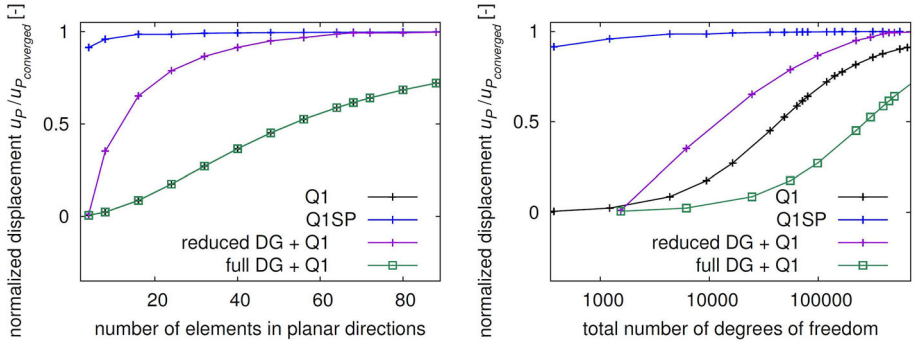

Fig. 13 Normalized vertical displacement of the point *P* in the thin plate as a function of the number of elements in each planar direction (left) and the total number of the degrees of freedom (right) for Q1, Q1SP, DG and their combinations with $\eta = 10^7$

Conclusions

A formulation of the discontinuous Galerkin method (IIPG) was introduced and later applied in five different 2D and 3D examples with a semi-analytical penalty parameter $\theta = \eta E/h$ [N/m^3]. This paper aimed at the investigation and comparison of the locking behavior of various continuous and discontinuous element types in both, volumetric (near incompressibility) and shear locking. Cook's membrane, a thin beam/plate bending, a 2D/3D block under compression were studied with the use of different elements, namely Q1, Q1SP, DG and their combinations. Discontinuous Galerkin elements neither showed significant volumetric nor shear locking. In all cases, the convergence of the discontinuous version of Q1 with either mixed or reduced integration improved significantly. However full integration of DG with Q1 element showed extreme locking. Eventually, the already satisfying performance of the continuous Q1SP could be improved by application of its discontinuous version.

Authors' contributions
All the authors contributed in the development and adaptation of the method for the current study. Bayat implemented the method in FEAP and performed the computations and drafted the manuscript. An element subroutine (Q1SP) from Reese was applied. Wulfinghoff and Reese supervised the study and corrected the manuscript draft. Kastian extended the work to 3D under Bayat's supervision. All authors read and approved the final manuscript.

Acknowledgements
Financial support of this work, related to the project "Hybrid discontinuous Galerkin methods in solid mechanics" from the priority program (SPP) 1748 funded by the German Science Foundation (DFG) is gratefully acknowledged.

Competing interests
The authors declare that they have no competing interests.

Availability of data and materials
Not applicable.

Consent for publication
Not applicable.

Ethics approval and consent to participate
Not applicable.

Funding
Not applicable.

Publisher's Note

Received: 6 June 2017 Accepted: 19 March 2018

References

1. Reed WH, Hill TR. Triangular mesh methods for the neutron transport equation. Los Alamos Report LA-UR-73-479. 1973.
2. Lesaint P, Raviart PA. On a finite element method for solving the neutron transport equation. In: Aziz AK, editor. Mathematical aspects of finite elements in partial differential equations. New York: Academic Press; 1974. p. 89–145.
3. Nitsche J. Über ein variationsprinzip zur lösung von dirichlet-problemen bei verwendung von teilräumen, die keinen randbedingungen unterworfen sind. In: Abhandlungen aus dem mathematischen Seminar der Universität Hamburg. vol. 36. Springer; 1971. p. 9–15.
4. Johnson C, Pitkäranta J. An analysis of the discontinuous Galerkin method for a scalar hyperbolic equation. Math Comput. 1986;46(173):1–26.
5. Brezzi F, Marini LD, Süli E. Discontinuous Galerkin methods for first-order hyperbolic problems. Math Models Methods Appl Sci. 2004;14(12):1893–903. https://doi.org/10.1142/S0218202504003866.
6. Johnson C. Discontinuous Galerkin finite element methods for second order hyperbolic problems. Comput Methods Appl Mech Eng. 1993;107(1):117–29.
7. Krivodonova L, Xin J, Remacle JF, Chevaugeon N, Flaherty JE. Workshop on innovative time integrators for PDEs shock detection and limiting with discontinuous Galerkin methods for hyperbolic conservation laws. Appl Numer Math. 2004;48(3):323–38. https://doi.org/10.1016/j.apnum.2003.11.002 ISSN 0168-9274.
8. Douglas J, Dupont T. Interior penalty procedures for elliptic and parabolic Galerkin methods. Berlin: Springer; 1976. p. 207–16. https://doi.org/10.1007/BFb0120591. ISBN 978-3-540-37550-0.
9. Wheeler MF. An elliptic collocation-finite element method with interior penalties. SIAM J Numer Anal. 1978;15(1):152–61.
10. Arnold DN. An interior penalty finite element method with discontinuous elements. SIAM J Numer Anal. 1982;19(4):742–60.
11. Baker GA, Jureidini WN, Karakashian OA. Piecewise solenoidal vector fields and the Stokes problem. SIAM J Numer Anal. 1990;27(6):1466–85.
12. Becker R, Hansbo P, Stenberg R. A finite element method for domain decomposition with non-matching grids. ESAIM Math Model Numer Anal. 2003;37(2):209–25.
13. Rusten T, Vassilevski P, Winther R. Interior penalty preconditioners for mixed finite element approximations of elliptic problems. Math Comput Am Math Soc. 1996;65(214):447–66.
14. Baker GA. Finite element methods for elliptic equations using nonconforming elements. Math Comput. 1977;31(137):45–59.
15. Bassi F, Rebay S. A high-order accurate discontinuous finite element method for the numerical solution of the compressible Navier-Stokes equations. J Comput Phys. 1997;131(2):267–79.

16. Cockburn B, Shu CW. The local discontinuous Galerkin method for time-dependent convection-diffusion systems. SIAM J Numer Anal. 1998b;35(6):2440–63.
17. Baumann CE, Oden JT. A discontinuous hp finite element method for convection—diffusion problems. Comput Methods Appl Mech Eng. 1999a;175(3):311–41.
18. Baumann CE, Oden JT. A discontinuous hp finite element method for the Euler and Navier-Stokes equations. Int J Numer Methods Fluids. 1999b;31(1):79–95.
19. Arnold DN, Brezzi F, Cockburn B, Marini LD. Unified analysis of discontinuous Galerkin methods for elliptic problems. SIAM J Numer Anal. 2002;39(5):1749–79.
20. Cockburn B, Karniadakis GE, Shu CW. The development of discontinuous Galerkin methods. In: Discontinuous Galerkin methods. Springer; 2000. p. 3–50.
21. Noels L, Radovitzky R. A general discontinuous Galerkin method for finite hyperelasticity. Formulation and numerical applications. Int J Numer Methods Eng. 2006;68(1):64–97.
22. Cockburn B, Shu CW. The Runge-Kutta discontinuous Galerkin method for conservation laws V. J Comput Phys. 1998a;141(2):199–224. https://doi.org/10.1006/jcph.1998.5892 ISSN 0021-9991.
23. Lomtev I, Karniadakis G. Simulations of viscous supersonic flows on unstructured hp-meshes. In: Proceedings of the 35th aerospace sciences meeting, Reno, Nevada; 1997.
24. Lomtev I, Quillen CB, Karniadakis G. Spectral/hp methods for viscous compressible flows on unstructured 2D meshes. J Comput Phys. 1998;144(2):325–57.
25. Cockburn B, Kanschat G, Schötzau D, Schwab C. Local discontinuous Galerkin methods for the Stokes system. SIAM J Numer Anal. 2002;40(1):319–43.
26. Cockburn B, Kanschat G, Schötzau D. The local discontinuous Galerkin method for the Oseen equations. Math Comput. 2004;73(246):569–93.
27. Warburton TC, Karniadakis G. A discontinuous Galerkin method for the viscous MHD equations. J Comput Phys. 1999;152(2):608–41.
28. Gremaud PA, Matthews JV. Simulation of gravity flow of granular materials in silos. In: Discontinuous Galerkin methods. Springer; 2000. p. 125–34.
29. Carranza FL, Haber RB. An adaptive discontinuous Galerkin model for coupled viscoplastic crack growth and chemical transport. In: Discontinuous Galerkin methods. Springer; 2000. p. 277–83.
30. Engel G, Garikipati K, Hughes TJR, Larson MG, Mazzei Luca, Taylor Robert L. Continuous/discontinuous finite element approximations of fourth-order elliptic problems in structural and continuum mechanics with applications to thin beams and plates, and strain gradient elasticity. Comput Methods Appl Mech Eng. 2002;191(34):3669–750.
31. Garth Wells N, Garikipati K, Molari L. A discontinuous Galerkin formulation for a strain gradient-dependent damage model. Comput Methods Appl Mech Eng. 2004;193(33):3633–45.
32. Molari L, Wells GN, Garikipati K, Ubertini F. A discontinuous Galerkin method for strain gradient-dependent damage: study of interpolations and convergence. Comput Methods Appl Mech Eng. 2006;195(13):1480–98.
33. Costanzo F, Huang H. Proof of unconditional stability for a single-field discontinuous Galerkin finite element formulation for linear elasto-dynamics. Comput Methods Appl Mech Eng. 2005;194(18):2059–76.
34. Huang H, Costanzo F. On the use of space-time finite elements in the solution of elasto-dynamic problems with strain discontinuities. Comput Methods Appl Mech Eng. 2002;191(46):5315–43.
35. Alberty J, Carstensen C. Discontinuous Galerkin time discretization in elastoplasticity: motivation, numerical algorithms, and applications. Comput Methods Appl Mech Eng. 2002;191(43):4949–68.
36. Mergheim J, Kuhl E, Steinmann P. A hybrid discontinuous Galerkin/interface method for the computational modelling of failure. Commun Numer Methods Eng. 2004;20(7):511–9.
37. Alipour A, Wulfinghoff S, Bayat HR, Svendsen B. The concept of control points in hybrid discontinuous Galerkin methods—application to geometrically nonlinear crystal plasticity. Int J Numer Methods Eng. 2018;114:557–79. https://doi.org/10.1002/nme.5754.nme.5754.
38. Hansbo P, Larson MG. Discontinuous Galerkin methods for incompressible and nearly incompressible elasticity by Nitsche's method. Comput Methods Appl Mech Eng. 2002a;191(17):1895–908.
39. Hansbo P, Larson MG. A discontinuous Galerkin method for the plate equation. Calcolo. 2002b;39(1):41–59.
40. Wihler T. Locking-free adaptive discontinuous Galerkin FEM for linear elasticity problems. Math Comput. 2006;75(255):1087–102.
41. Di Pietro DA, Nicaise S. A locking-free discontinuous Galerkin method for linear elasticity in locally nearly incompressible heterogeneous media. Appl Numer Math. 2013;63:105–16.
42. Ten Eyck A, Lew A. Discontinuous Galerkin methods for non-linear elasticity. Int J Numer Methods Eng. 2006;67(9):1204–43.
43. Celiker F, Cockburn B, Stolarski HK. Locking-free optimal discontinuous Galerkin methods for timoshenko beams. SIAM J Numer Anal. 2006;44(6):2297–325.
44. Wulfinghoff S, Bayat HR, Alipour A, Reese S. A low-order locking-free hybrid discontinuous Galerkin element formulation for large deformations. Comput Methods Appl Mech Eng. 2017;323(Supplement C):353–72 ISSN 0045-7825.
45. Reese S, Küssner M, Reddy BD. A new stabilization technique for finite elements in non-linear elasticity. Int J Numer Methods Eng. 1999;44(11):1617–52.
46. Reese S. On the equivalent of mixed element formulations and the concept of reduced integration in large deformation problems. Int J Nonlinear Sci Numer Simul. 2002;3(1):1–34.
47. Reese S. On a consistent hourglass stabilization technique to treat large inelastic deformations and thermo-mechanical coupling in plane strain problems. Int J Numer Methods Eng. 2003;57(8):1095–127.
48. Reese S, Wriggers P. A stabilization technique to avoid hourglassing in finite elasticity. Int J Numer Methods Eng. 2000;48(1):79–109.
49. Reese S, Bayat HR, Wulfinghoff S. On an equivalence between a discontinuous Galerkin method and reduced integration with hourglass stabilization for finite elasticity. Comput Methods Appl Mech Eng. 2017;325(Supplement C):175–97. https://doi.org/10.1016/j.cma.2017.07.005. ISSN 0045-7825.

50. Reese S, Wriggers P, Reddy BD. A new locking-free brick element technique for large deformation problems in elasticity. Comput Struct. 2000;75(3):291–304. https://doi.org/10.1016/S0045-7949(99)00137-6 ISSN 0045-7949.
51. Fritz A, Hüeber S, Wohlmuth BI. A comparison of mortar and Nitsche techniques for linear elasticity. Calcolo. 2004;41(3):115–37.
52. Taylor RL. FEAP-finite element analysis program. University of California, Berkeley. 2014. http://www.ce.berkeley/feap.